

Total acoustic transmission between fluids using a solid material with emphasis on the air-water interface

Hesam Bakhtiary Yekta¹ and Andrew N. Norris

*Department of Mechanical and Aerospace Engineering,
Rutgers University, Piscataway, NJ 08854, USA*

(Dated: February 12, 2025)

Abstract

Total acoustic transmission between water and air is modeled using a purely solid interface comprising two elastic plates separated by periodically spaced ribs. The frequency of full transmission depends only on, and is inversely proportional to, the areal density of the plate facing the air. Total transmission also requires a specific dependence of the rib spacing on the bending stiffness of the two plates. These relations are the result of an explicit analytical solution for the transmitted and reflected acoustic waves combined with asymptotic approximations based on the small parameter defined by the air-to-water impedance ratio. Surprisingly, the total transmission effect is almost independent of the angle of incidence, even though the transmission conditions are predicated on normal incidence. Parametric studies are performed to examine the effect on the frequency bandwidth and Q-factor of the acoustic transmissivity. A lower bound for the Q-factor of 30.6 is simply related to the water-air impedance ratio.

I. INTRODUCTION

In a 1942 US patent, Hansell [1] first described how impedance matching between acoustic fluids can be achieved by a quarter wavelength intermediate layer with impedance equal to the harmonic mean of the two media. The layer results in zero reflection and total energy transmission. Hansell also suggested a two layer solution, also quarter wavelength, with each impedance the harmonic mean of its neighbors; the goal of introducing two or more layers is to increase the bandwidth of the single layer device. Hansell’s ideas saw little immediate application in acoustics; rather, the focus of impedance matching in the mid-20th century was on microwave transformers, with a comprehensive body of literature, e.g. [2]. A later acoustics related application of impedance layers emerged for piezoelectric transducers in contact with air or water. In this case, the finite thickness of the piezoelectric element should be considered leading to, for instance, a single layer impedance $Z_{\text{air}}^{2/3} Z_{\text{piezo}}^{1/3}$ [3]. Here we are concerned with energy transmission between semi-infinite acoustic media so that Hansell’s single layer impedance is appropriate [1]. The difficulty lies in finding the specific material with the desired intermediate impedance. In particular, no naturally occurring material has the required impedance for the air-water interface.

Recent interest in impedance matching between air and water has been prompted by the innovative approach of Bok et al. [4] that employs an air layer as a spring in series with a membrane mass. This and most other proposed methods require air-water interfaces either through membranes [4], bare bubbles [5–8], bubbles within a membrane [9], hydrophobic materials [10], lotus acoustic metasurface [11], air channels [12], metal inclusions in air and in water [13]. Another proposed method uses airborne radar to measure the water surface acoustic displacement [14]. Other approaches include [15, 16] which uses a layer of 3D printed epoxy designed via topology optimization to have impedance equal to the harmonic mean of water and air, and transmission at a ”fish scale” resonance [17].

We present a simple acoustic impedance matching mechanism for the water-air interface. The matching layer, or transformer, is made from a solid material, e.g. aluminum. No fluid layers, either water or air, membranes or other mechanisms are required. Unlike the other proposed transformers including the solid ones [15, 16, 18] the present approach is analytically explicit, with closed form expressions relating the performance characteristics, e.g. transmission frequency, to the material properties. This allows us to find remarkably

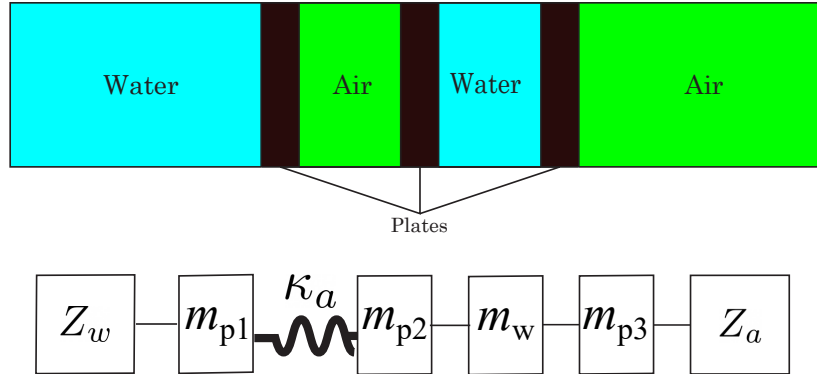


FIG. 1. A spring-mass resonator separating semi-infinite water on the left and air on the right. The air layer acts as the spring κ_a , and the water layer is a mass m_w . The dividing thin plates add masses m_{p1}, m_{p2} , and m_{p3} , to the system.

simple relations by taking advantage of the asymptotically small parameter defined by the ratio of the air and water acoustic impedances.

By way of introduction to the problem we begin in Section II with a simple but fundamental transformer model motivated by the ideas of Bok et al. [4] and others [10, 13]. In the process we show why models with air-water interfaces are very difficult to realize in practice. The flex-layer impedance transformer is presented in Section III along with a summary of the main results. Mathematical details are given in Section IV, and the conditions for total transmission are derived in Section V. The efficacy of the proposed model is demonstrated in Section VI along with discussion of factors such as the effect of entrained air between the plates, and concluding with a comparison with the fundamental one-dimensional model presented next. A summary and conclusions are given in Section VII.

II. A SIMPLE WATER-TO-AIR IMPEDANCE MATCHING USING WATER AND AIR LAYERS

The acoustic properties of air and water are characterized by densities, ρ_a, ρ_w , and bulk moduli K_a, K_w , with derived quantities, sound speed $c = \sqrt{K/\rho}$ and impedance $Z = \sqrt{K\rho}$. Figure 1 depicts the model: semi-infinite bodies of water and air surround a transformer comprising thin layers of air and water, with thin plates separating them as **w|a|w|a**. The central **|a|w|** transformer has mass elements m_{p1}, m_{p2}, m_{p3} , and m_w for the plates and the

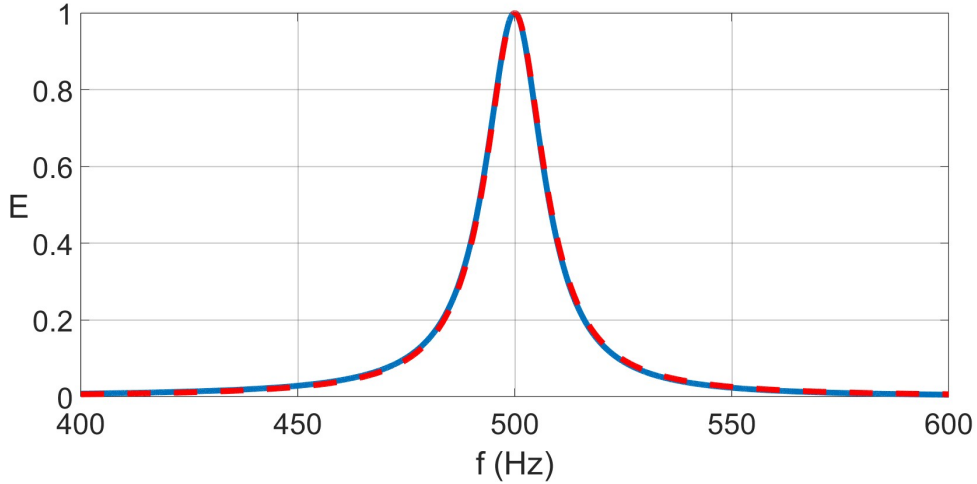


FIG. 2. Transmitted energy for unit incident energy from the water side, $f_0 = 500$ Hz. Solid curve is a full wave (exact) simulation and the dashed curve is the asymptotic approximation $E \approx 1 / \left(1 + \frac{1}{\epsilon} \left(\frac{f}{f_0} - 1\right)^2\right)$. The latter follows from the lumped-parameter impedance of Eq. (1) as $E = 1 - |R|^2$ for reflection coefficient $R = \frac{Z - Z_w}{Z + Z_w}$.

water layer, and spring element κ_a for the air layer. Assuming time dependence $e^{-i\omega t}$ with $\omega = 2\pi f$, the effective impedance of the transformer in series with the semi-infinite air can be calculated using low frequency lumped parameters models [19] as

$$Z = -i\omega m_{p1} + \left\{ (Z_a - i\omega m)^{-1} - i\omega \kappa_a^{-1} \right\}^{-1} \quad (1)$$

where $m = m_w + m_{p2} + m_{p3}$. The condition for impedance matching to water, $Z = Z_w + 0i$, becomes, taking $m_{p1} = 0$ for simplicity since it acts only as a phase term in water,

$$\kappa_a m = Z_w Z_a, \quad \text{and} \quad \omega \approx \omega_0 \equiv \frac{\sqrt{Z_w Z_a}}{m}. \quad (2)$$

Condition (2)₁ says the transformer impedance $\sqrt{\kappa_a m}$ is the geometric mean of Z_w and Z_a in agreement with Hansell [1]. Condition (2)₂ follows from the exact solution $\omega = \omega_0 (1 - \epsilon)^{1/2}$ based on asymptotics for the small parameter

$$\epsilon \equiv \frac{Z_a}{Z_w} = 0.267 \times 10^{-3}, \quad (3)$$

and shows that full transmission is at the resonance frequency $\omega_0 = \sqrt{\kappa_a/m}$.

Figure 2 shows a full wave simulation using transfer matrices for three 1 mm thick Al plates. Dissipation in the air layer from viscous and thermal diffusivity is included [20] with

no evident influence. Two curves are plotted, solid and dotted: the latter is an asymptotic approximation for the transmitted energy in air based on the lumped parameter model, $E \approx 1/\left(1 + \frac{1}{\epsilon}\left(\frac{f}{f_0} - 1\right)^2\right)$. Its remarkable accuracy indicates how there are no adjustable quantities in the response, even though we have built free parameters into the design. This simple formula for E says that the Q -factor of the transmission resonance, which arises from radiation damping, not from energy dissipation, has a characteristic value of $Q \approx \frac{1}{2\sqrt{\epsilon}} = 30.6$. We will return to this value later in §VI B.

Introduce effective thicknesses d_a and d_w for air and water according to

$$\kappa_a = \frac{\rho_a c_a^2}{d_a}, \quad m = \rho_w d_w, \quad (4)$$

then (2) translates to the equivalent conditions

$$\frac{\omega_0 d_a}{c_a} = \sqrt{\epsilon}, \quad \frac{d_w}{c_w} = \frac{d_a}{c_a}. \quad (5)$$

The fact that $\sqrt{\epsilon} = 0.016$ justifies the subwavelength approximations. While the thickness of the effective water layer is adjustable, based on the choice of the plates which provide mass, the thickness of the air layer is severely limited by the fact that it is the only stiffness operating, and Eq. (5)₁ constrains it as $d_a = 0.87/f_0$ m at f_0 Hz transmission frequency. This requires plate separation d_a on the order of 1 mm at 870 Hz and less for higher f_0 which seems hard to imagine over large areas in water. Placing spacers between the air plates would keep the plates separated, but adds stiffness in parallel which requires d_a to be further decreased. This is not a feasible solution since any parallel stiffness would overwhelm the air stiffness. While it is instructive, the simple model of Fig. 1 is impractical.

An alternative approach is discussed next which replaces the fluid **|a|w|** transformer with a purely solid *flex layer*.

III. PROBLEM SETUP AND SUMMARY OF THE MAIN RESULTS

The impedance transformer is motivated by the fact that a pair of parallel elastic plates in water and separated by periodically spaced ribs, a "flex-layer", acts at low frequency as an equivalent stiffness [21]. This contrasts with the usual low frequency approximation of an elastic solid as a mass, leading to the well known mass-law transmission loss [22, Sec. 6.7]. The effective stiffness of the flex-layer offers an alternative to the air-layer stiffness of

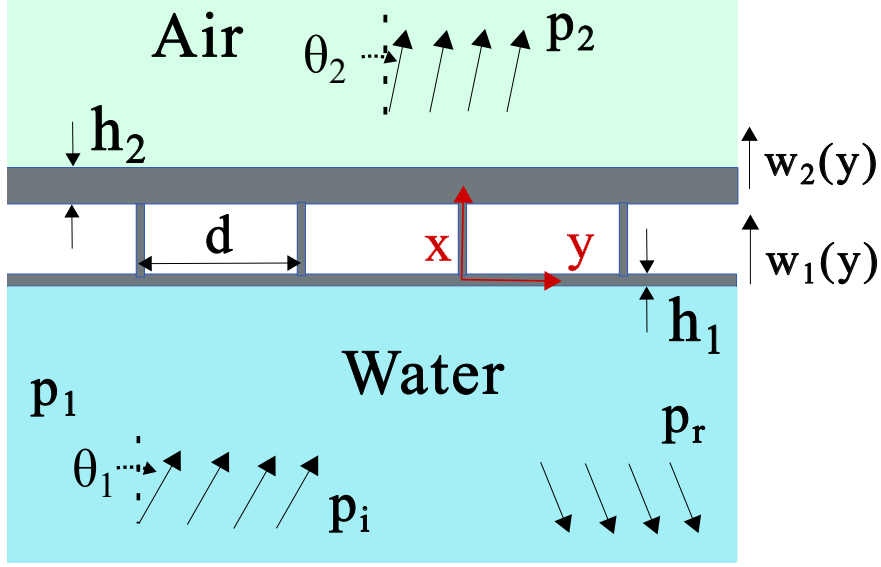


FIG. 3. A plane wave is incident from the water side of the asymmetric panel. The plates are separated by ribs set a distance d apart with the intermediate space assumed to be vacuum. The effect of entrained air is small and is discussed in Section VID.

the simple model of Fig. 1, while the mass of the plates provides the necessary mass for the transmission resonance. The flex-layer considered here may have two distinct plates, but as we will see, only the one facing the air contributes to the effective mass of the resonator.

A. The flex-layer impedance transformer

The transformer layer is depicted in Fig. (3). The semi-infinite water and air regions occupy $x < 0$ and $x > 0$, respectively (the finite gap between the plates is compressed into a single point for simplicity). We label water and air quantities with subscripts 1 and 2, respectively, so that the wavenumbers are $k_j = \omega/c_j$ where c_j are the sound speeds, and for later ρ_j are the densities. We consider plane wave incidence in water at angle θ_1 from the normal, with y -wavenumber $k_0 = k_1 \sin \theta_1$. The fundamental transmitted wave in air is at angle θ_2 which follows from Snell's law: $k_2 \sin \theta_2 = k_1 \sin \theta_1$, and hence $\theta_2 \leq \theta_1$.

The impedance matching system comprises two parallel plates of thickness h_1 and h_2 separated by periodically spaced ribs, see Fig. 3. The plate parameters are mass per unit area $m_j = \rho_{sj}h_j$ and bending stiffness $D_j = E_j I_j / (1 - \nu_j^2)$ where $I_j = \frac{h_j^3}{12}$, $j = 1, 2$.

B. Principal results

Here we summarize the main results that define the conditions required for total transmission under normal incidence ($\theta_j = 0, j = 1, 2$). The first condition necessary for full transmission relates the transmission frequency ω_0 to the mass densities m_1, m_2 , and the acoustic impedances $Z_j = \rho_j c_j, j = 1, 2$:

$$Z_1 + \frac{m_1^2 \omega_0^2}{Z_1} = Z_2 + \frac{m_2^2 \omega_0^2}{Z_2}, \quad (6)$$

see §V A and Appendix B. For the water-air interface $Z_1 = Z_w, Z_2 = Z_a$, this reduces to

$$\omega_0 \approx \frac{\sqrt{Z_w Z_a}}{m_2} \quad (7)$$

which is precise if $m_1 = m_2$ and is otherwise less than 0.1% in error. It is interesting to compare this with the condition $(2)_2$ for the simple model of Fig. 1, which also depends upon the mass facing the air half-space.

The second condition involves solving for the zero of a nonlinear function, although the solution can be approximated (see Section VI) for the air-water interface by a relation similar to $(2)_1$ for the simple transformer model

$$\kappa m_2 \approx Z_a Z_w \quad \text{where} \quad \kappa = \frac{720}{d^4} \left(\frac{1}{D_1} + \frac{1}{D_2} \right)^{-1}. \quad (8)$$

In practice, (8) provides the condition for determining the rib spacing d that yields full transmission at $\omega = \omega_0$ of (7). In summary, the flex-layer acts as a spring-mass transformer with stiffness κ that depends on the stiffness of both plates and mass $m = m_2$ that depends only on the mass of the plate on the air side.

IV. SCATTERING ANALYSIS FOR AN ASYMMETRIC PANEL

On the water side, plate 1 $x < 0$, we consider the incident acoustic pressure p_i along with its rigidly reflected pressure, which together give zero normal velocity on the plate. The plate normal velocity, $v_1(y) = v_x(-0, y)$ is therefore related to the additional pressure p_1 by the momentum equilibrium equation in the x -direction: $i\omega\rho_1 v_1(y) = \frac{\partial p_1}{\partial x}(0, y)$. On the air side the total acoustic pressure $p = p_2$ radiates away from the plate in the positive x -direction, and the plate normal velocity, $v_2(y) = v_x(+0, y)$, is given by $i\omega\rho_2 v_2(y) =$

$\frac{\partial p_2}{\partial x}(0, y)$. Introducing the y -transforms,

$$\hat{V}_j(\xi) = \int_{-\infty}^{\infty} v_j(y) e^{-i\xi y} dy, \quad v_j(y) = \frac{1}{2\pi} \int_{-\infty}^{\infty} \hat{V}_j(\xi) e^{i\xi y} d\xi, \quad j = 1, 2, \quad (9)$$

it follows that the additional scattered pressure in the water ($j = 1$) and the total pressure in the air ($j = 2$) are related to the normal velocities by

$$p_j(x, y) = \frac{\text{sgn } x}{2\pi} \int_{-\infty}^{\infty} \hat{Z}_{fj}(\xi) \hat{V}_j(\xi) e^{i(\sqrt{k_j^2 - \xi^2} |x| + \xi y)} d\xi, \quad j = 1, 2 \quad (10)$$

with fluid impedances

$$\hat{Z}_{fj}(\xi) = \frac{\rho_j \omega}{\sqrt{k_j^2 - \xi^2}}, \quad j = 1, 2. \quad (11)$$

The square roots in eqs. (10) and (11) are either positive real or positive imaginary. In summary, the total pressure in water ($x < 0$) and air ($x > 0$) is

$$p(x, y) = \begin{cases} p_1(x, y) + p_0 e^{i k_1 (x \cos \theta_1 + y \sin \theta_1)} + p_0 e^{i k_1 (-x \cos \theta_1 + y \sin \theta_1)}, & x < 0, \\ p_2(x, y), & x > 0, \end{cases} \quad (12)$$

with p_1 and p_2 given by eq. (10).

A. Solution

The displacements of plates 1 and 2 in the x -direction, $w_j(y) = (-i\omega)^{-1} v_j(y)$, satisfy

$$\mathcal{L}_1 w_1(y) = 2p_0 e^{i k_0 y} + p_1(0, y) - \left[Z_{0+}(v_2 + v_1)(y) - Z_{0-}(v_2 - v_1)(y) \right] \sum_{l=-\infty}^{\infty} \delta(y - ld), \quad (13a)$$

$$\mathcal{L}_2 w_2(y) = -p_2(0, y) - \left[Z_{0+}(v_2 + v_1)(y) + Z_{0-}(v_2 - v_1)(y) \right] \sum_{l=-\infty}^{\infty} \delta(y - ld), \quad (13b)$$

where $\mathcal{L}_j w(y) = D_j w''''(y) - m_j \omega^2 w(y)$, $j = 1, 2$. The stiffness impedance Z_{0-} defines the force between the plates that depends on their relative separation, while Z_{0+} is a mass impedance that depends on the motion of the rib center of mass. For simplicity in the equations, it is assumed that the ribs make point contacts with the plates as their thicknesses are negligible in comparison with the plate length. Two models for $Z_{0\pm}$ are given in Appendix A. Substituting the Poisson summation identity [23, 24]

$$\sum_{l=-\infty}^{\infty} \delta(y - ld) = \frac{1}{d} \sum_{m=-\infty}^{\infty} e^{-i 2\pi m \frac{y}{d}} \quad (14)$$

and taking the ξ transform of (13a) and (13b) gives

$$\begin{aligned}\hat{V}_1(\xi) &= -(q_+(\xi) - q_-(\xi)) \hat{Y}_1(\xi) + 4\pi p_0 \hat{Y}_1(k_0) \delta(\xi - k_0), \\ \hat{V}_2(\xi) &= -(q_+(\xi) + q_-(\xi)) \hat{Y}_2(\xi),\end{aligned}\tag{15}$$

where

$$q_{\pm}(\xi) = \frac{Z_{0\pm}}{d} \sum_{m=-\infty}^{\infty} (\hat{V}_2(\xi + \frac{2\pi m}{d}) \pm \hat{V}_1(\xi + \frac{2\pi m}{d})),\tag{16}$$

with admittances

$$\hat{Y}_j(\xi) = \{\hat{Z}_{pj}(\xi) + \hat{Z}_{fj}(\xi)\}^{-1}, \quad j = 1, 2,\tag{17}$$

and plate impedances

$$\hat{Z}_{pj}(\xi) = \frac{D_j \xi^4 - m_j \omega^2}{-i\omega}, \quad j = 1, 2.\tag{18}$$

The latter are based on the Kirchhoff plate theory. Mindlin plate theory is an alternative and arguably more accurate model, but from related work [21] it is not expected to provide a noticeable difference.

Noting that the functions q_{\pm} are periodic, $q_{\pm}(\xi) = q_{\pm}(\xi + \frac{2\pi m}{d})$ for integer m , it follows from Eqs. (15) and (16) that

$$\begin{pmatrix} q_+(\xi) \\ q_-(\xi) \end{pmatrix} = \frac{4\pi p_0 \hat{Y}_1(k_0)}{1 + (\frac{d}{Z_{0+}} - \frac{d}{Z_{0-}}) \hat{Z}_0(k_0)} \begin{pmatrix} \hat{Z}_+(k_0) + 2\hat{Z}_0(k_0) \\ -\hat{Z}_-(k_0) \end{pmatrix} \sum_{m=-\infty}^{\infty} \delta(\xi - k_0 - \frac{2\pi m}{d})\tag{19}$$

where

$$\begin{aligned}\hat{Z}_-(\xi) &= \left\{ \frac{d}{Z_{0-}} + 2\hat{S}_1(\xi) \right\}^{-1}, \\ \hat{Z}_+(\xi) &= \left\{ \frac{d}{Z_{0+}} + 2\hat{S}_2(\xi) \right\}^{-1}, \\ \hat{Z}_0(\xi) &= \hat{Z}_+(\xi) \hat{Z}_-(\xi) (\hat{S}_2(\xi) - \hat{S}_1(\xi))\end{aligned}\tag{20}$$

and

$$\hat{S}_j(\xi) = \sum_{m=-\infty}^{\infty} \hat{Y}_j(\xi + \frac{2\pi m}{d}), \quad j = 1, 2.\tag{21}$$

B. Reflected and transmitted waves

Equations (10), (15) and (19) together yield the scattered pressure on either side,

$$\begin{aligned}p_j(x, y) &= 2p_0 \hat{A}_j(k_0) \sum_{m=-\infty}^{\infty} \hat{Z}_{fj}(\xi_m) \hat{Y}_j(\xi_m) e^{i((-1)^j (k_{1x})_m x + \xi_m y)} \\ &\quad - 2p_0 \hat{Z}_{f1}(k_0) \hat{Y}_1(k_0) e^{k_1(-x \cos \theta_1 + y \sin \theta_1)} \delta_{j1}, \quad j = 1, 2,\end{aligned}\tag{22}$$

where

$$\hat{A}_1(\xi) = \frac{(\hat{Z}_+(\xi) + \hat{Z}_-(\xi) + 2\hat{Z}_0(\xi))}{1 + \left(\frac{d}{Z_{0+}} - \frac{d}{Z_{0-}}\right)\hat{Z}_0(\xi)} \hat{Y}_1(\xi), \quad \hat{A}_2(\xi) = \frac{\hat{Z}_+(\xi)\hat{Z}_-(\xi)\hat{Y}_1(\xi)}{\left(\frac{d}{Z_{0+}} - \frac{d}{Z_{0-}}\right)^{-1} + \hat{Z}_0(\xi)}, \quad (23)$$

and

$$\xi_m = k_0 + 2\pi\frac{m}{d}, \quad (k_{jx})_m = \sqrt{k_j^2 - \xi_m^2} \quad \text{for } m \in \mathbb{Z}. \quad (24)$$

We assume that only the fundamental $m = 0$ scattered modes propagate in air and water. All other Bragg wavenumbers in the x direction, $(k_{jx})_m$, $m \neq 0$, are positive imaginary, leading to evanescent acoustic fields. For normal incidence this requires that $k_2 < 2\pi/d$ or equivalently $fd/c_a < 1$. The value of fd/c_a does not exceed 0.2 in the numerical examples discussed below.

Total pressure in the incident water ($x < 0$) and the transmitted medium air ($x > 0$) follows from Eqs. (12) and (22) as

$$p(x, y) = \begin{cases} p_0 e^{i k_1 (x \cos \theta_1 + y \sin \theta_1)} + p_0 R(\theta_1) e^{i k_1 (-x \cos \theta_1 + y \sin \theta_1)} + p_{1ev}(x, y), & x < 0, \\ p_0 T(\theta_2) e^{i k_2 (x \cos \theta_2 + y \sin \theta_2)} + p_{2ev}(x, y), & x > 0, \end{cases} \quad (25)$$

where

$$\begin{aligned} R(\theta_1) &= R_1(\theta_1) + (1 - R_1(\theta_1)) \hat{A}_1(k_0), \\ T(\theta_2) &= (1 - R_2(\theta_2)) \hat{A}_2(k_0), \end{aligned} \quad (26)$$

R_1 and R_2 are the reflection coefficient for plane wave incidence on the plates,

$$R_j(\theta_j) = \frac{\hat{Z}_{pj}(k_0) - \hat{Z}_{fj}(k_0)}{\hat{Z}_{pj}(k_0) + \hat{Z}_{fj}(k_0)}, \quad (27)$$

and the evanescent, or near, fields, are

$$p_{jev}(x, y) = 2p_0 \hat{A}_j(k_0) \sum_{m \neq 0} \hat{Z}_{fj}(\xi_m) \hat{Y}_j(\xi_m) e^{i((k_{jx})_m |x| + \xi_m y)}. \quad (28)$$

Energy conservation requires that

$$|R|^2 + \frac{Z_w \sec \theta_1}{Z_a \sec \theta_2} |T|^2 = 1. \quad (29)$$

Note that the reflection coefficient can be expressed in the alternative form

$$R(\theta_1) = \frac{\hat{Z}'_{p1}(k_0) - \hat{Z}_{f1}(k_0)}{\hat{Z}'_{p1}(k_0) + \hat{Z}_{f1}(k_0)} \quad (30)$$

suggestive of reflection from a plate with impedance

$$\hat{Z}'_{p1}(\xi) = \hat{Z}_{p1}(\xi) + \frac{\hat{A}_1(\xi)}{(1 - \hat{A}_1(\xi))\hat{Y}_1(\xi)}. \quad (31)$$

V. CONDITIONS FOR FULL TRANSMISSION

Total transmission corresponds to $R = 0$, implying two conditions for the real and imaginary parts. In order to understand these conditions we consider the case of rigid and massless ribs. This has little effect on the full solution, as we will see, but it significantly simplifies the algebra, allowing us to find the necessary constraints on the system parameters.

A. Frequency for total transmission

In the limit that the ribs are rigid, $1/Z_{0-} \rightarrow 0$, and massless, $Z_{0+} \rightarrow 0$: $\hat{A}_1(\xi) = \hat{A}_2(\xi) = \hat{Y}_1(\xi)/(\hat{S}_1(\xi) + \hat{S}_2(\xi))$ and the reflection coefficient takes the form

$$R(\theta_1) = \frac{R_1(\theta_1) \Gamma(k_0)}{\hat{S}_1(k_0) + \hat{S}_2(k_0)} \quad (32)$$

where

$$\Gamma(k_0) = \hat{S}'_1(k_0) + \hat{S}'_2(k_0) + \frac{1}{\hat{Z}_{p1}(k_0) - \hat{Z}_{f1}(k_0)} + \frac{1}{\hat{Z}_{p2}(k_0) + \hat{Z}_{f2}(k_0)} \quad (33)$$

with $\hat{S}'_j(\xi) = \hat{S}_j(\xi) - \hat{Y}_j(\xi)$, $j = 1, 2$. Total transmission corresponds to zero reflection, and we therefore look at the conditions required to make Γ and hence R vanish. We consider normal incidence, $k_0 = 0$.

Under these circumstances $\hat{S}'_1(k_0)$ and $\hat{S}'_2(k_0)$ are imaginary. Setting the real part of $\Gamma(0)$ in (33) to zero yields the transmission frequency ω_0 :

$$\omega_0^2 = \frac{Z_w Z_a (Z_w - Z_a)}{Z_w m_2^2 - Z_a m_1^2}. \quad (34)$$

Equivalently,

$$\omega_0 = \frac{\sqrt{Z_w Z_a}}{m_2} \left(\frac{1 - \epsilon}{1 - \epsilon m_1^2/m_2^2} \right)^{1/2} \quad (35)$$

where $\epsilon \ll 1$ is defined in (3). This provides the remarkable simplification

$$\omega_0 \approx \frac{Z_e}{m_2} \quad \text{where} \quad Z_e \equiv \sqrt{Z_w Z_a}, \quad (36)$$

which is a very accurate approximation to Eq. (35) on account of the smallness of ϵ .

An alternative and simpler method is presented in Appendix B for finding the frequency of full transmission, Eq. (34).

B. Optimal rib spacing

Setting the imaginary part of $\Gamma(k_0)$ of (33) to zero at $\omega = \omega_0$ given by (36), with $k_0 = 0$ yields

$$2 \sum_{n=1}^{\infty} \left\{ \left(\hat{D}_1 n^4 - \frac{m_1}{m_2} - \frac{\rho_w d}{m_2 2\pi n} \right)^{-1} + \left(\hat{D}_2 n^4 - 1 \right)^{-1} \right\} \approx 1 \quad (37)$$

where $\hat{D}_j = \frac{m_2 (2\pi)^4}{Z_e^2 d^4} D_j$, $j = 1, 2$ and the approximations $\epsilon \ll 1$ and $\rho_a d / m_2 \ll 1$ have been used. Equation (37) determines d for chosen h_1 , or *vice versa*. For instance, if ω_0 and h_1 are chosen, along with the plate materials (e.g. both aluminum), then Eq. (36) defines h_2 and (37) determines d .

Equation (37) has a close connection with the quasistatic stiffness of the two-plate flex-layer [21] as we now explain. Ignoring the inertial terms, which is consistent with the quasistatic limit, (37) becomes

$$2 \sum_{n=1}^{\infty} \left\{ \left(\hat{D}_1 n^4 \right)^{-1} + \left(\hat{D}_2 n^4 \right)^{-1} \right\} \approx 1 \quad \Rightarrow \quad d \approx d_0 \quad (38)$$

where

$$d_0^4 = \frac{720}{Z_e \omega_0} \left(\frac{1}{D_1} + \frac{1}{D_2} \right)^{-1} \quad (39)$$

and the identity $\sum_{n=1}^{\infty} \frac{1}{n^4} = \frac{\pi^4}{90}$ has been used. The relation (38)₂ for d can be understood in terms of the effective quasistatic stiffness κ_{eff} of the flex-layer introduced in [21] for a symmetric plate system. In the present case the plates are different and we need to take the flexural stiffness of the plates in series, i.e. $\kappa_{\text{eff}} = (\kappa_1^{-1} + \kappa_2^{-1})^{-1}$ where $\kappa_j = 720 D_j / d^4$ [21]. The connection with (38)₂ follows from the resonance condition $\kappa_{\text{eff}} = m \omega_0^2$ for effective mass $m = m_2$. Together with (36) this yields $\kappa_{\text{eff}} = Z_e \omega_0$ which then implies the relation for d according to (38)₂.

Assuming h_1 is chosen, then d follows approximately from the estimate d_0 of Eq. (39). We use d_0 as an initial estimate for the solution of the nonlinear equation (37).

VI. NUMERICAL DEMONSTRATIONS AND DISCUSSION

Illustrative examples are presented based on the derived equations in sections IV and V. In all cases both plates are Aluminum ($\rho_s = 2,700 \text{ kg/m}^3$, $E = 70 \text{ GPa}$, $\nu = 0.334$), and the thickness of plate 1 is $h_1 = 1 \text{ mm}$. The theoretical equations are verified by

numerical simulation, using COMSOL with the multi-physics options set to "2-D Acoustic-Solid Interaction, Frequency Domain" using "Perfectly Matched Boundary" and "Periodic Condition" on the model boundaries. The ribs are assumed to be infinitely stiff, with a length of 1 cm and a thickness of 1 mm.

A. Full transmission

Full transmission at a given frequency f_0 requires that the lengths h_2 and d assume optimal values according to Eqs. (36) and (37). We proceed by choosing the transmission frequency f_0 , then find $h_2 \approx Z_e/(2\pi f_0 \rho_{s2})$ from Eq. (36) and subsequently use this value to find d from Eq. (37), with the initial guess $d = d_0$ of Eq. (39).

We consider three different flex-layers with parameters based on the optimal values of d and h_2 for normal incidence ($\theta_1 = 0^\circ$) at transmission frequencies $f_0 = 250$ Hz ($d = 9.5$ cm and $h_2 = 5.78$ mm), $f_0 = 500$ Hz ($d = 7.58$ cm and $h_2 = 2.89$ mm), and $f_0 = 1000$ Hz ($d = 5.89$ cm and $h_2 = 1.44$ mm). Figure 4 shows the transmitted acoustic energy $E = \frac{z_w \sec \theta_1}{z_a \sec \theta_2} |T|^2$ for both normal incidence and for incident angles $\theta_1 = 10^\circ$ and $\theta_1 = 30^\circ$. It is evident from Fig. 4 that the optimal h_2 and d for normal incidence also work for oblique incidence, and that the full-transmission frequency is independent of θ_1 for a given optimized flex-layer. Simulations based on the theory assumes that the rib mass and thickness are negligible. These assumptions can lead to slight deviations between the simulation and COMSOL results at higher frequencies, as for example, in Fig. 4 for the 1000-Hz case.

Figure 5 illustrates the relation between f_0 , h_2 , and d for a range of transmission frequencies. The values of the approximate spacing d_0 is also shown, indicating that it is an overestimate of the optimal spacing for the parameter range considered. The optimal h_2 and d in Fig. 5 are calculated for normal incidence $\theta_1 = 0^\circ$. Based on the results of Fig. 4 we can safely surmise that the same optimal values apply for $\theta_1 \neq 0^\circ$.

B. Bandwidth and Q-factor

We consider the effect of some system parameters on the bandwidth of the acoustic transmissivity. The parametric studies are conducted in such a way that if the same resonant frequency is desired, then changing the parameters of the first plate also changes d to

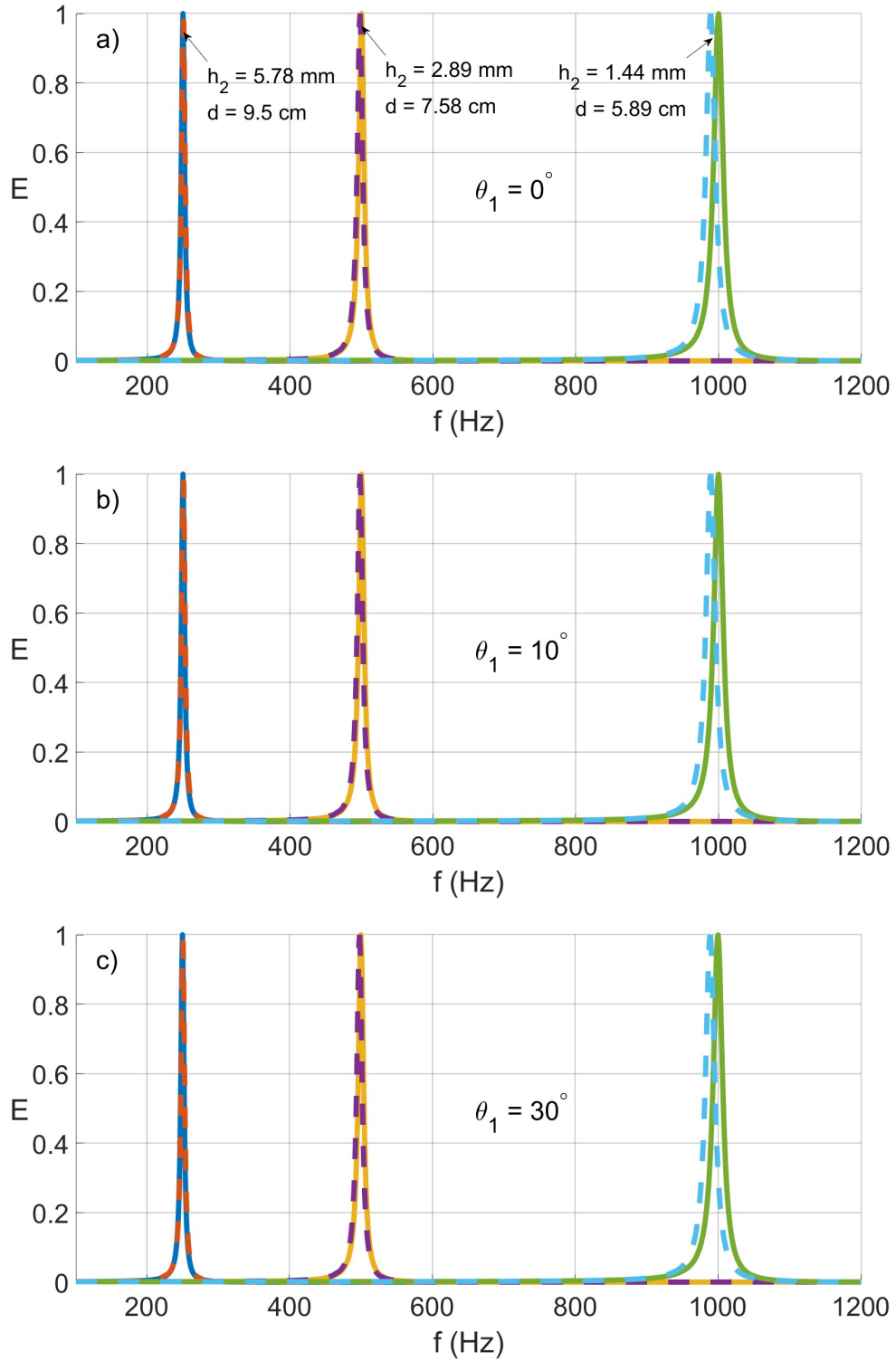


FIG. 4. The transmitted acoustic energy E vs frequency for the flex-layer model based on optimal values obtained for a) $\theta_1 = 0^\circ$, b) $\theta_1 = 10^\circ$ and c) $\theta_1 = 30^\circ$. Dashed lines are obtained using COMSOL. In all cases $h_1 = 1$ mm.

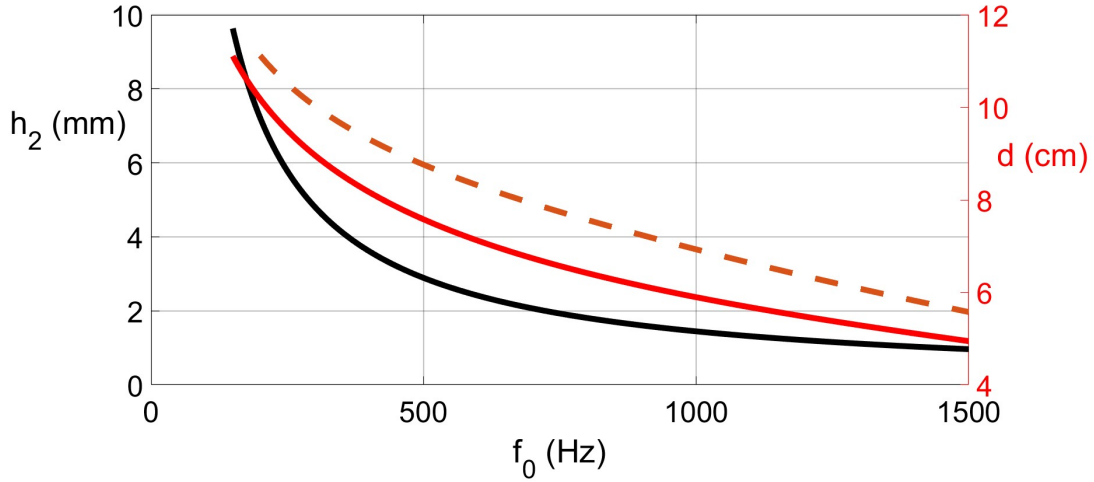
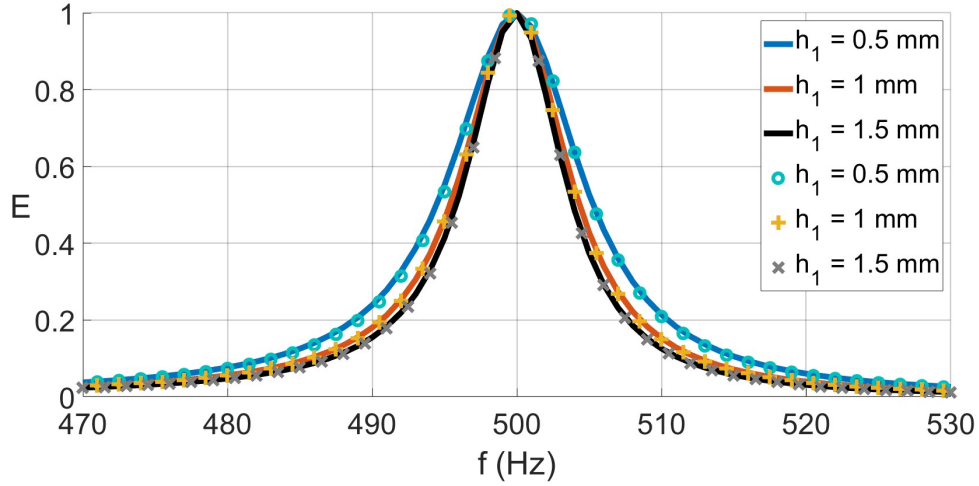


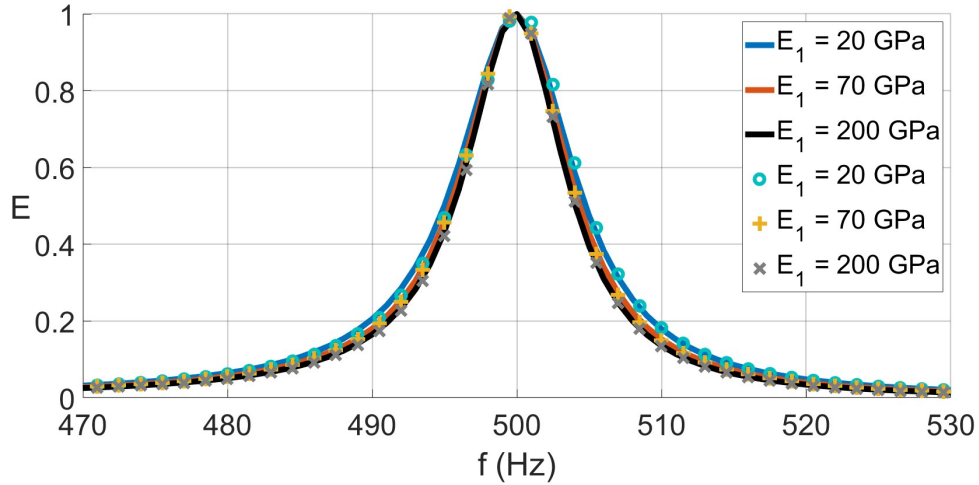
FIG. 5. Optimal values for h_2 and d vs f_0 for normal incidence. $h_1 = 1$ mm. The dashed curve is the approximation d_0 of Eq. (39).

maintain the equivalent bending stiffness of the first plate. We focus on full transmission at $f_0 = 500$ Hz. Thus, for the case that $h_1 = 1$ mm, the optimal value for d is 7.58 cm, while for $h_1 = 0.5$ and 1.5 mm, the optimal values for d are 4.75 cm and 9.86 cm, respectively). The results demonstrate that h_1 has an inverse relationship with the bandwidth. Consequently, by decreasing h_1 , the bandwidth increases, as depicted in Fig. 6(a). The next parameter we investigated to observe its effect on the bandwidth is the Young's modulus of the first plate, E_1 . As shown in Fig. 6(b), E_1 exhibits an inverse relationship with the bandwidth (for the case that $E_1 = 70$ GPa, the optimal value for d is 7.58 cm, while for $E_1 = 20$ and 200 GPa, the optimal values for d are 5.69 cm and 9.58 cm, respectively). By comparing Figs. 6(a) and 6(b), it is evident that the effect of h_1 on the bandwidth is stronger than E_1 .

Finally, the frequency bandwidth (BW) and Q-factor for the acoustic transmission are studied, where $Q = \frac{f_0}{\Delta f}$ with Δf equal to the BW at $E = \frac{1}{2}$. As illustrated in Fig. 7, the Q-factor decreases with decreasing h_1 , converging to $\frac{1}{2\sqrt{\epsilon}} \approx 30.6$, where $\epsilon = Z_a/Z_w$. From the results in Figs. 6(a) and 7, it is observed that by decreasing h_1 , the result converges to the simple model of Fig. 2, where the Q-factor and bandwidth were found to be 30.6 and 16.34 Hz, respectively.



(a) Effect of varying h_1 with $E_1 = 70$ GPa



(b) Effect of varying E_1 with $h_1 = 1$ mm

FIG. 6. The effect of varying bending stiffness parameters for plate 1. The solid curves are theory and the symbolic shapes \circ , $+$, and \times are COMSOL results.

C. Motion of the plates

In order to further understand the mechanics at play in the full transmission effect it is instructive to consider the motion of plates 1 and 2 facing water and air, respectively. At total transmission the energy fluxes of the incident and transmitted waves are equal. Assuming 1D propagation (as in the model of Section II), implies $p_1 v_1 = p_2 v_2$. Using the plane wave relations $p_1 = Z_w v_1$ and $p_2 = Z_a v_2$ it follows that $v_1 = \pm \sqrt{\epsilon} v_2$ with ϵ defined in (3). We now discuss whether or not this relation is reflected in the numerical simulations.

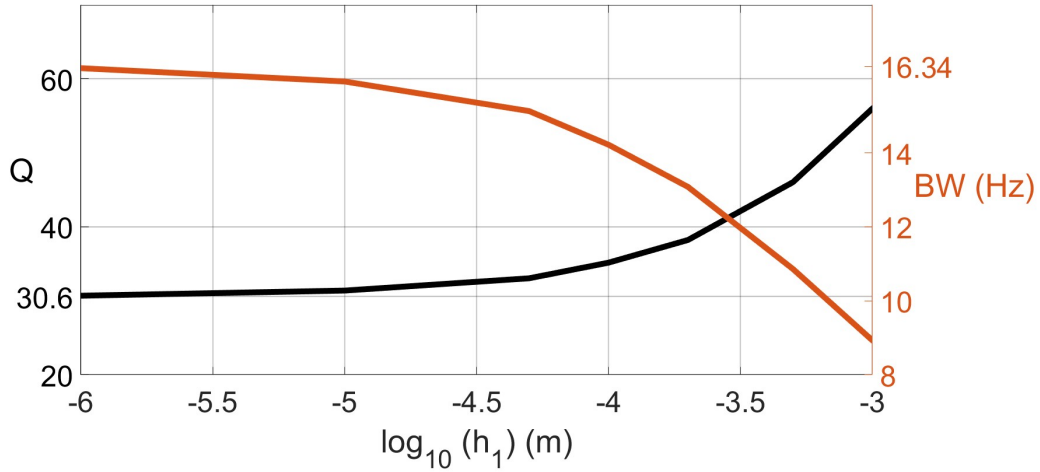


FIG. 7. The effect of varying h_1 on the Q-factor and BW.

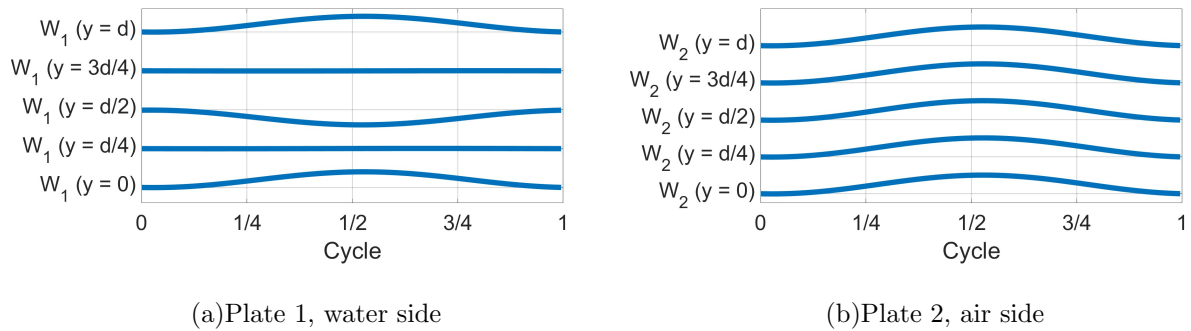


FIG. 8. The plate displacements $w_1(t)$ and $w_2(t)$ over a cycle, $0 \leq f_0 t \leq 1$ for $f_0 = 500$ Hz. The data is from the video Video 2, $f_0 = 500$ Hz.

The short summary is that it is approximately, but in an averaged sense. The longer story requires some explanation.

Figure 8 shows the plate displacements over one cycle for transmission frequency $f_0 = 500$ Hz. It is clear that plate 2 on the air side moves like a plane wave, but the same is not true for plate 1. The dramatic difference in the plate motions is better appreciated from the associated videos for three transmission frequencies: Video 1, $f_0 = 250$ Hz, Video 2, $f_0 = 500$ Hz, and Video 3, $f_0 = 1000$ Hz. To better understand the dramatically different plate dynamics, we refer to Appendix B which derives an alternative and simpler method for finding the frequency of full transmission, Eq. (34). The method uses spatial averages of the plate displacements, \bar{w}_1 and \bar{w}_2 . In addition to the frequency condition Eq. (34) it also follows from Eq. (B6) that the average motion of plate 1 small in comparison to that

of plate 2, i.e. $\bar{w}_1 \approx -i\sqrt{\epsilon}\bar{w}_2$.

We therefore have different expectations: $\bar{w}_1 \approx \eta\sqrt{\epsilon}\bar{w}_2$ where η can be $-i$, $+1$ or -1 . We find from simulation (COMSOL) that $\frac{\bar{w}_1}{\sqrt{\epsilon}\bar{w}_2}$ takes the values $1.319 e^{-0.53 i \frac{\pi}{2}}$, $1.65 e^{-0.36 i \frac{\pi}{2}}$, $1.52 e^{-0.445 i \frac{\pi}{2}}$ for $f_0 = 250$ Hz, 500 Hz and 1000 Hz, respectively. We conclude that none of the above are correct, although the magnitude is close, $|\bar{w}_1| \approx \sqrt{\epsilon}|\bar{w}_2|$, indicating very little average motion of plate 1. The difference can be ascribed to the assumptions used in Appendix B, specifically that the pressure and velocity on plate 1 are related by the plane wave impedance relation $p_1 = Z_w \bar{v}_1$, which is clearly not the case. Near-field evanescent effects are important at plate 1 but are not included in the analysis of Appendix B.

Finally, we note that the mode shape of plate 1 on the water side can be accurately modeled if we ignore the effect of fluid loading and consider the plate equation only. The mode must be symmetric in y with zero slope at $y = \pm \frac{d}{2}$, and hence

$$w_1(y) = C_1 \left[\sinh\left(\frac{\beta d}{2}\right) \cos(\beta y) + \sin\left(\frac{\beta d}{2}\right) \cosh(\beta y) \right] \quad (40)$$

where $\beta^4 = \omega_0^2 m_1 / D_1$. We assume that the shear force at $y = \pm \frac{d}{2}$ is approximately zero, i.e. $D_1 w_1'''(\pm \frac{d}{2}) \approx 0$, implying $\sin(\frac{\beta d}{2}) \approx 0$. Taking the first non trivial solution, $\beta \approx \frac{2\pi}{d}$, yields the simple mode shape

$$w_1(y) \approx A_1 \cos\left(\frac{2\pi}{d}y\right) \quad (41)$$

for some A_1 . Figure 9 indicates remarkable agreement between the light fluid loading model of Eq. (41) and COMSOL simulations of the water-facing plate.

D. Effect of air between the plates

We consider how the assumption of vacuum between the plates compares with the more realistic scenario of entrained air. The presence of air introduces an equivalent spring between the plates with stiffness κ_a similar to that in Section II. In this case $\kappa_a = \rho_a c_a^2 / L_r$ where L_r is the rib length, i.e. the distance separating the plates. Also, based upon the previous results for the plate motions, it is expected that the relative displacement $\bar{w}_2 - \bar{w}_1$ is well approximated by \bar{w}_2 . Therefore, as a first approximation we assume that the effect of the air is to change the effective acceleration of plate 2 from $-m_2 \omega^2 w_2$ to approximately $-(m_2 \omega^2 - \kappa_a) w_2$. Using this in the derivation of (34) from (32) yields a transmission fre-

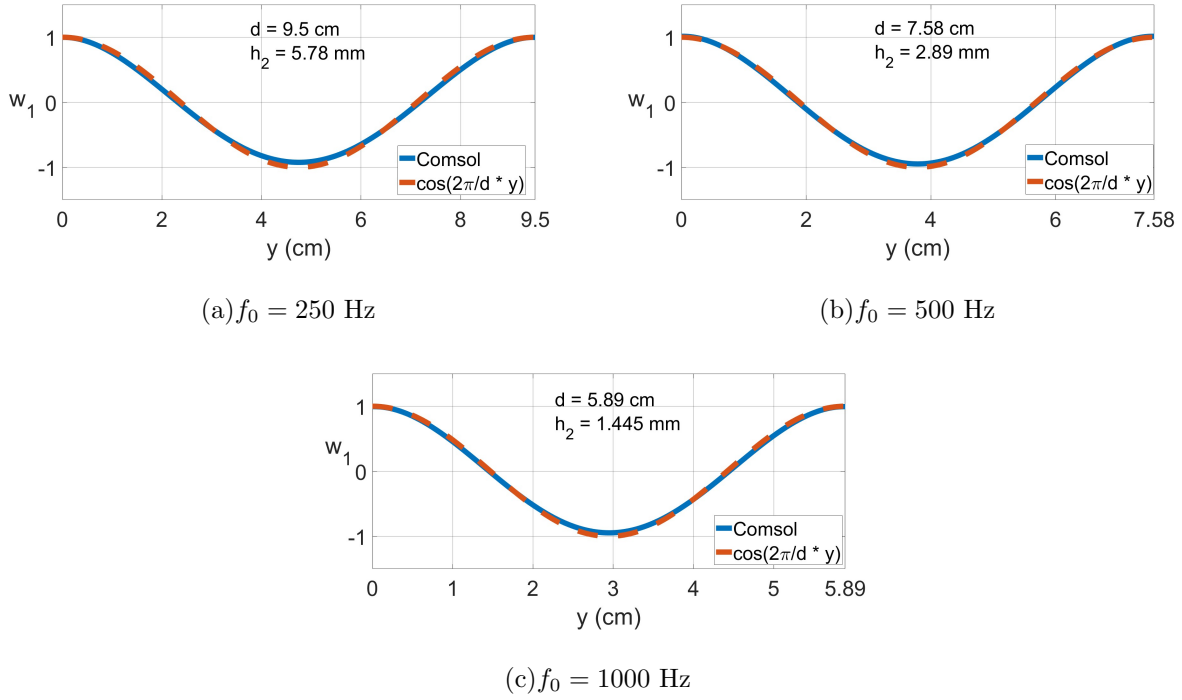


FIG. 9. The mode shape of plate 1 facing water at full transmission for three transmission frequencies: 250 Hz, 500 Hz and 1000 Hz.

quency ω greater than ω_0 of Eq. (7) which satisfies

$$m_2^2 \omega^4 - (Z_w Z_a + 2m_2 \kappa_a) \omega^2 + \kappa_a^2 \approx 0. \quad (42)$$

Hence

$$\frac{\omega}{\omega_0} \approx \frac{1}{2} + \sqrt{\frac{1}{4} + \frac{\sqrt{\epsilon}}{\lambda}} \quad \text{where} \quad \lambda = \frac{\omega_0 L_r}{c_a}. \quad (43)$$

The dependence on transmission frequency and rib length combine in the single non-dimensional parameter λ .

Figure 10 demonstrates that Eq. (43) accurately predicts the effect of the presence of air on the flex-layer transmission frequency. In particular, the frequency shows an inverse relationship with the length of the ribs, indicating that shorter rib lengths result in stronger spring characteristics of the air. The resonant frequency increases as the air volume decreases and κ_a increases. However, by taking L_r sufficiently long, on the order a centimeter such that $\lambda \gg \sqrt{\epsilon}$, the effect of the air is negligible and the vacuum model is adequate.

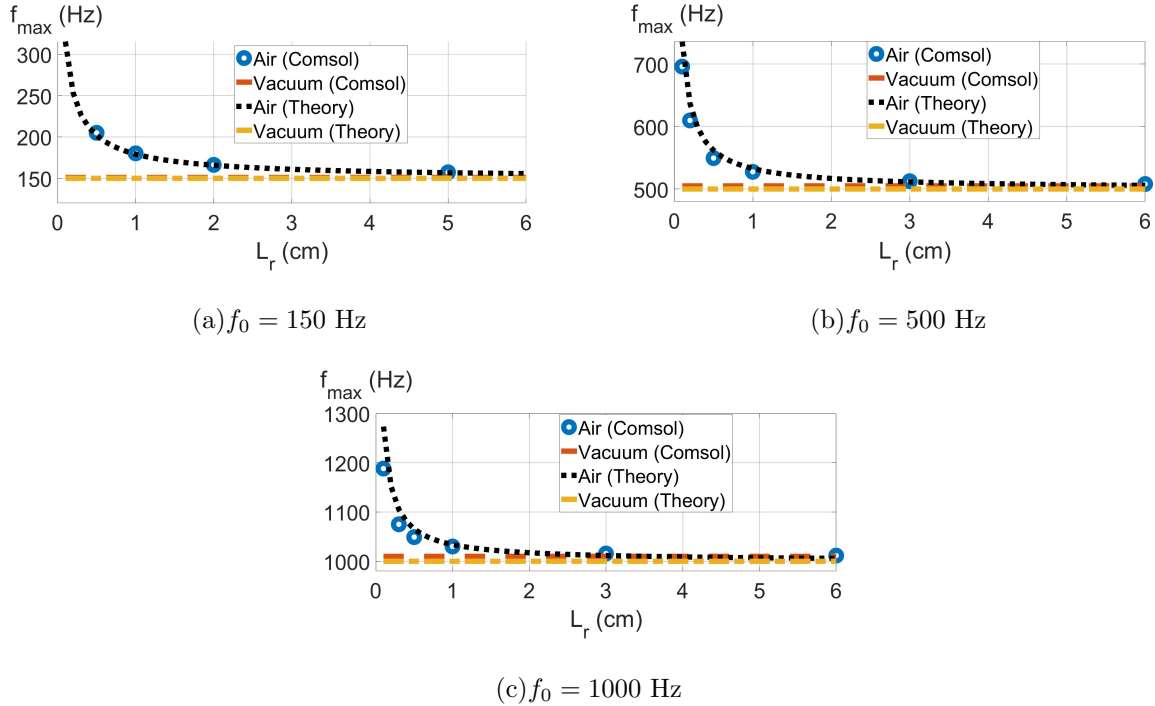


FIG. 10. The effect of air between the plates as a function of the rib length L_r for three full transmission frequencies: (a) $f_0 = 150$ Hz, (b) $f_0 = 500$ Hz, (c) $f_0 = 1000$ Hz.

VII. SUMMARY AND CONCLUSIONS

We have presented a straightforward method to obtain the impedance matching between two acoustic fluids, with the primary emphasis, in this paper, on the water-air interface. The matching layer, or transformer, is achieved by using a solid material like aluminum with no active power source, fluid layers, membranes, or any other passive mechanism. Different from other proposed transformers, including solid ones, the approach in this paper is analytically explicit, resulting in closed-form expressions that relate the performance characteristics, such as the transmission frequency, directly to the material properties or dimensions of the flex-layer. The proposed flex-layer acts as an impedance transformer if the system parameters are chosen according to explicit criteria. Thus, for a given transmission frequency $\omega_0 = 2\pi f_0$ the areal density m_2 of the plate facing air must satisfy Eq. (7). This defines the required thickness of the plate. A second relation, Eq. (37), defines the required rib spacing d , with d_0 of Eq. (39) an approximate over-estimate. The analytic nature of the acoustic scattering solution along with asymptotic approximations based on $\epsilon = \frac{Z_a}{Z_w} \ll 1$ leads to explicit expressions such as Eq. (7) and to physical understanding such as the quite distinct motions

of the two plates, described in Section VI C. It also allows us to compare the flex-layer model with a simple spring-mass transformer defined by an effective mass m_2 and effective stiffness κ of Eq. (8).

Comparisons of the analytic solution for total transmission shows excellent agreement with full wave simulations, including for oblique incidence even though the system parameters are chosen to give full transmission for normal incidence, Fig. 4. The effect of air between the plates it to increase the effective stiffness and increase the transmission frequency from that for a vacuum, with the simple approximation of Eq. (43) in good agreement with full wave simulations. The bandwidth of the transmission resonance depends upon the free system parameters, such as the thickness of the plate facing water. A parametric study indicates that the Q-factor has a lower achievable limit of $\frac{1}{2\sqrt{\epsilon}} = 30.6$, the same as the Q-factor for the ideal spring-mass model of Section II. A reduction of the Q-factor, and associated larger bandwidth, is the subject of a separate study on an alternative transformer model.

Appendix A: Plate equations from Hamilton's principle

The plate equations (13a) and (13b) are derived here using Hamilton's principle

$$\delta \int L \, dt = \delta \int (T - U + W) \, dt = 0 \quad (\text{A1})$$

with Lagrangian elements defined by the real-valued displacements and pressure according to

$$\begin{aligned} T &= T_- + T_+ + T_{\text{rib}}, & T_{\pm} &= \int \frac{1}{2} \rho_{\pm} h_{\pm} \omega^2 w_{\pm}^2 \, dy, \\ U &= U_- + U_+ + U_{\text{rib}}, & \text{where } U_{\pm} &= \int \frac{1}{2} D_{\pm} w_{\pm,yy}^2 \, dy, \\ W &= W_- + W_+, & W_{\pm} &= \mp \int p_{\pm} w_{\pm} \, dy. \end{aligned} \quad (\text{A2})$$

Here \pm indicates the contributions from the plates on $x = \pm 0$. The integrals are over a single period in the y -direction that includes one rib between the plates at $y = 0$. This formulation considers the rib as an internal member, and all external forces are contained in the W_{\pm} terms.

The terms T_{rib} and U_{rib} are defined by the rib model, and they depend on the plate displacements at $y = 0$, that is $w_{\pm}(0)$. Taking the variation of (A1) with respect to w_{\pm}

yields

$$\rho_{\pm} h_{\pm} \omega^2 w_{\pm} - D_{\pm} w_{\pm,yyyy} \mp p_{\pm} + \frac{\partial(T_{\text{rib}} - U_{\text{rib}})}{\partial w_{\pm}(0)} \delta(y - 0) = 0. \quad (\text{A3})$$

We consider two rib models that allow us to express $(T_{\text{rib}} - U_{\text{rib}})$ in terms of w_+ and w_- .

1. A mass-spring rib model

The rib is a mass m with springs of stiffness 2κ on either side that attach to the plates, so the static effective stiffness is κ . This introduces the mass degree of freedom, u , its displacement in the x -direction, and

$$T_{\text{rib}} = \frac{1}{2} m \omega^2 u^2, \quad U_{\text{rib}} = \frac{1}{2} 2\kappa [(u - w_-(0))^2 + (u - w_+(0))^2]. \quad (\text{A4})$$

Variation of (A1) with respect to the rib mass displacement u leads to

$$m\omega^2 u + 2\kappa(w_+(0) + w_-(0) - 2u) = 0. \quad (\text{A5})$$

Using this to eliminate u gives

$$T_{\text{rib}} - U_{\text{rib}} = \frac{\kappa}{2} \left[\frac{m\omega^2}{4\kappa - m\omega^2} (w_+(0) + w_-(0))^2 - (w_+(0) - w_-(0))^2 \right]. \quad (\text{A6})$$

The plate equations (13) then follow from (A3) with

$$Z_{0-} = \frac{\kappa}{-i\omega}, \quad Z_{0+} = \frac{-i\omega\kappa m}{4\kappa - m\omega^2}. \quad (\text{A7})$$

2. The continuous rib model

The rib is a plate in tension/compression with parameters ρ and E located between $x = -L/2$ and $x = L/2$. The time harmonic displacement is

$$u(x) = (w_+(0) + w_-(0)) \frac{\cos kx}{2 \cos k\frac{L}{2}} + (w_+(0) - w_-(0)) \frac{\sin kx}{2 \sin k\frac{L}{2}} \quad (\text{A8})$$

where $k = \omega/c$, $c = \sqrt{E/\rho}$, and

$$T_{\text{rib}} = \int_{-\frac{L}{2}}^{\frac{L}{2}} \frac{1}{2} \rho h \omega^2 u^2 dx, \quad U_{\text{rib}} = \int_{-\frac{L}{2}}^{\frac{L}{2}} \frac{1}{2} E h u_{,x}^2 dx. \quad (\text{A9})$$

Hence,

$$T_{\text{rib}} - U_{\text{rib}} = \frac{1}{4} k h E \left[(w_+(0) + w_-(0))^2 \tan k\frac{L}{2} - (w_+(0) - w_-(0))^2 \cot k\frac{L}{2} \right], \quad (\text{A10})$$

and the plate equations (13) follows from (A3) with impedances

$$Z_{0-} = i\rho c \frac{h}{2} \cot \frac{kL}{2}, \quad Z_{0+} = -i\rho c \frac{h}{2} \tan \frac{kL}{2}. \quad (\text{A11})$$

These are consistent with the spring-mass model for $\kappa = \frac{Eh}{L}$ and $m = \rho hL$, as expected for the low frequency regime. Note that $Z_{0-}Z_{0+} = (\rho c \frac{h}{2})^2$ which is independent of frequency.

Appendix B: Alternative derivation of the transmission frequency

We provide a simple and alternative route to the relation (34) for the frequency at full transmission. The derivation does not use infinite sums or explicit solutions in the acoustic media, but relies on the plate equations only.

Consider a unit period of the layer, Fig. (3). Assume the pressure p_2 in the fluid above the layer, air, acts as a plane wave with particle averaged velocity \bar{v}_2 where $p_2 = Z_a \bar{v}_2$. At total transmission the pressure p_1 in the water below the layer is also a wave in one direction because of zero reflection, and accordingly $p_1 = Z_w \bar{v}_1$. We also include the air between the plates which acts as a spring of stiffness $\kappa_a \approx \frac{\rho_a c_a^2}{L_r}$ due to the compressibility of the air, where L_r is the plate spacing [21]. The plate equations are then

$$D_j w_j''''(y) - m_j \omega^2 w_j = (-1)^j [-Z_j \bar{v}_j + \kappa_a (\bar{w}_1 - \bar{w}_2)], \quad j = 1, 2, \quad (\text{B1})$$

where $Z_1 = Z_w$, $Z_2 = Z_a$. Using $v = -i\omega w$ yields

$$w_j(y) = w_j^{(0)} u_j(y) + \frac{(-1)^j}{\omega^2 m_j} [-i\omega Z_j \bar{w}_j + \kappa_a (\bar{w}_2 - \bar{w}_1)], \quad j = 1, 2, \quad (\text{B2})$$

where $u_j(y)$ are solutions to the homogeneous equations (B1) normalized such that $u_j(\frac{d}{2}) = 1$. Note, we do not know the precise form of these solutions since the force acting at the rib at $y = \frac{d}{2}$ is unknown, except for the fact the forces are equal and opposite on the two ribs. However, we can still find a useful result without knowing u_1 and u_2 .

The solutions (B2) satisfy two conditions. The first is the kinematic constraint $w_1(\frac{d}{2}) = w_2(\frac{d}{2})$ implying

$$w_1^{(0)} + \frac{i\omega Z_w \bar{w}_1 + \kappa_a (\bar{w}_1 - \bar{w}_2)}{\omega^2 m_1} = w_2^{(0)} + \frac{-i\omega Z_a \bar{w}_2 + \kappa_a (\bar{w}_2 - \bar{w}_1)}{\omega^2 m_2}. \quad (\text{B3})$$

The displacements $w_j^{(0)}$ can be related to \bar{w}_j by taking the average of (B2), so that (B3) becomes

$$\left[\frac{i\omega Z_w}{m_1} \left(1 - \frac{1}{\bar{u}_1}\right) + \frac{\omega^2}{\bar{u}_1} + \frac{\kappa_a \gamma}{m_1 m_2} \right] \bar{w}_1 + \left[\frac{i\omega Z_a}{m_2} \left(1 - \frac{1}{\bar{u}_2}\right) - \frac{\omega^2}{\bar{u}_2} - \frac{\kappa_a \gamma}{m_1 m_2} \right] \bar{w}_2 = 0 \quad (\text{B4})$$

where

$$\gamma = m_1 + m_2 - \frac{m_1}{\bar{u}_2} - \frac{m_2}{\bar{u}_1}. \quad (\text{B5})$$

The second condition is that the shear forces acting at the ribs are equal and opposite: $D_1 w_1'''(\frac{d}{2}) + D_2 w_2'''(\frac{d}{2}) = 0$. The latter is equivalent, by integration from 0 to $\frac{d}{2}$, to taking the average of the sum of the two equations (B1), i.e.

$$(Z_w + i\omega m_1) \bar{w}_1 = (Z_a - i\omega m_2) \bar{w}_2. \quad (\text{B6})$$

Equations (B4) and (B6) are then a pair of linear and homogeneous equations in \bar{w}_1 and \bar{w}_2 . In order that non-trivial solutions are possible the determinant must be zero, i.e.

$$\begin{aligned} & \left(\frac{Z_w}{m_1} - \frac{Z_a}{m_2} \right) \omega^2 \gamma - (Z_w - Z_a) \left(\omega^2 + \frac{\kappa_a \gamma}{m_1 m_2} \right) \\ & + i\omega \left\{ \left(\omega^2 + \frac{Z_a Z_w}{m_1 m_2} \right) \gamma - (m_1 + m_2) \left(\omega^2 + \frac{\kappa_a \gamma}{m_1 m_2} \right) \right\} = 0. \end{aligned} \quad (\text{B7})$$

The transmission frequency ω_0 follows from (B7) in the same form as (34), independent of the air layer stiffness κ_a . Note that γ also follows from (B7).

In summary, the identity (34) has been deduced using a lumped parameter model combined with the plate equations for one spatial period.

-
- [1] Hansell CW. 1942 Impedance matching means for mechanical waves. US Patent 2,430,013.
 - [2] Southworth GC. 1950 *Principles and Application of Waveguide Transmission*. D. Van Nostrand Co., Inc., New York, N. Y.
 - [3] Desilets C, Fraser J, Kino G. 1978 The design of efficient broad-band piezoelectric transducers. *IEEE Transactions on Sonics and Ultrasonics* **25**, 115–125. (10.1109/t-su.1978.31001)
 - [4] Bok E, Park JJ, Choi H, Han CK, Wright OB, Lee SH. 2018 Metasurface for Water-to-Air Sound Transmission. *Phys. Rev. Lett.* **120**, 044302. (10.1103/physrevlett.120.044302)
 - [5] Bretagne A, Tourin A, Leroy V. 2011 Enhanced and reduced transmission of acoustic waves with bubble meta-screens. *Applied Physics Letters* **99**, 221906. (10.1063/1.3663623)
 - [6] Bolghasi A, Ghadimi P, Chekab MAF. 2017 Low-frequency sound transmission through rough bubbly air-water interface at the sea surface. *Journal of Low Frequency Noise, Vibration and Active Control* **36**, 319–338. (10.1177/1461348417744295)

- [7] Cai Z, Zhao S, Huang Z, Li Z, Su M, Zhang Z, Zhao Z, Hu X, Wang Y, Song Y. 2019 Bubble Architectures for Locally Resonant Acoustic Metamaterials. *Advanced Functional Materials* **29**. (10.1002/adfm.201906984)
- [8] Lee T, Iizuka H. 2020 Sound propagation across the air-water interface by a critically coupled resonant bubble. *Physical Review B* **102**, 104105. (10.1103/physrevb.102.104105)
- [9] Gong XT, Zhou HT, Zhang SC, Wang YF, Wang YS. 2023 Tunable sound transmission through water-air interface by membrane-sealed bubble metasurface. *Applied Physics Letters* **123**. (10.1063/5.0171461)
- [10] Huang Z, Zhao S, Zhang Y, Cai Z, Li Z, Xiao J, Su M, Guo Q, Zhang C, Pan Y, Cai X, Song Y, Yang J. 2021a Tunable Fluid-Type Metasurface for Wide-Angle and Multifrequency Water-Air Acoustic Transmission. *Research* **2021**. (10.34133/2021/9757943)
- [11] Huang Z, Zhao Z, Zhao S, Cai X, Zhang Y, Cai Z, Li H, Li Z, Su M, Zhang C, Pan Y, Song Y, Yang J. 2021b Lotus Metasurface for Wide-Angle Intermediate-Frequency Water-Air Acoustic Transmission. *ACS Applied Materials* **13**, 53242–53251. (10.1021/acsami.1c16043)
- [12] Liu J, Li Z, Liang B, Cheng J, Alù A. 2023 Remote Water-to-Air Eavesdropping with a Phase-Engineered Impedance Matching Metasurface. *Advanced Materials* **35**. (10.1002/adma.202301799)
- [13] Zhou P, Jia H, Bi Y, Yang Y, Zhang P, Yang J. 2023 Gradient Impedance Matching Layers Enable Broadband Water-Air Sound Transmission. Arxiv eprint 2305.07896. .
- [14] Tonolini F, Adib F. 2018 Networking across boundaries. In *Proceedings of the 2018 Conference of the ACM Special Interest Group on Data Communication* pp. 117–131. ACM. (10.1145/3230543.3230580)
- [15] Zhou HT, Zhang SC, Zhu T, Tian YZ, Wang YF, Wang YS. 2023 Hybrid Metasurfaces for Perfect Transmission and Customized Manipulation of Sound Across Water-Air Interface. *Advanced Science*. (10.1002/advs.202207181)
- [16] Zhang SC, Zhou HT, Gong XT, Wang YF, Wang YS. 2024 Discrete metasurface for extreme sound transmission through water-air interface. *Journal of Sound and Vibration* **575**, 118269. (10.1016/j.jsv.2024.118269)
- [17] Esposito A, Tallarico D, Sayed Ahmed M, Miniaci M, Shahab S, Bergamini A. 2024 Bioinspired Fano-like resonant transmission: frequency selective impedance matching. *Journal of Physics D: Applied Physics* **57**, 155402. (10.1088/1361-6463/ad1c86)

- [18] Zhou P, Jia H, Bi Y, Yang Y, Yang Y, Zhang P, Yang J. 2023 Water–air acoustic communication based on broadband impedance matching. *Applied Physics Letters* **123**. (10.1063/5.0168562)
- [19] Blackstock DT. 2001 *Fundamentals of physical acoustics*. Acoustical Society of America.
- [20] Lighthill J. 1978 *Waves in Fluids*. Cambridge University Press.
- [21] Bakhtiary Yekta H, Norris AN. 2024 Analytical solutions for single and multiple scattering from rib-stiffened plates in water. *The Journal of the Acoustical Society of America* **155**, 2247–2256. (10.1121/10.0025388)
- [22] Kinsler LE, Frey AR, Coppens AB, Sanders JV. 2000 *Fundamentals of Acoustics*. Wiley fourth edition.
- [23] Evseev V. 1973 Sound radiation from an infinite plate with periodic inhomogeneities. *Soviet Physics Acoustics -USSR* **19**, 226–229.
- [24] Lin GF, Garrelick JM. 1977 Sound transmission through periodically framed parallel plates. *The Journal of the Acoustical Society of America* **61**, 1014–1018. (10.1121/1.381386)